Desalination and Water Treatment
www.deswater.com
doi: 10.1080/19443994.2013.769660

51 (2013) 4302–4312
June

Taylor & Francis
Taylor & Francis Group

Influence of crossflow microfiltration on ceramic membrane fouling and beer quality

Mohammad Amin Kazemi[a], Mohammad Soltanieh[a,*], Mehdi Yazdanshenas[b] Luc Fillaudeau[c]

[a]*Chemical and Petroleum Engineering Department, Sharif University of Technology, Azadi Avenue, P.O. Box 111 55 9694 Tehran, Iran*
Tel. +98 21 6616 5417; Fax: +98 21 6602 2853; email: msoltanieh@sharif.edu
[b]*Department of Research and Development of Iran Behnoush Co, Tehran, Iran*
[c]*Université de Toulouse, Laboratoire d'Ingénierie des Systèmes Biologiques et des Procédés, CNRS UMR5504, INRA UMR792, INSA, 135, avenue de Rangueil, F-31077 Toulouse, France*

Received 31 August 2011; Accepted 29 April 2012

ABSTRACT

In this article, an experimental investigation has been carried out to determine the types of fouling phenomena that occur during clarification of dilute malt extract (DME) and pasteurization of clarified beer (CB) by a tubular ceramic membrane in a crossflow pilot plant. Using the classical models, the predominant fouling mechanism responsible for flux decline was found to be complete blocking of the membrane pores followed by formation of a compressible cake layer of yeast cell in the case of DME clarification, whereas the internal fouling of the membrane occurs during pasteurization of CB. The effects of operating parameters, including temperature, transmembrane pressure, and crossflow velocity, on the steady-state permeate flux, as the key factor of crossflow microfiltration processes, were examined. For CB microfiltration, the steady-state permeation flux increased almost linearly with transmembrane pressure and the membrane could reduce the turbidity by 60%. For DME filtration, the maximum value of permeation flux (20 LMH) was obtained under medium transmembrane pressure of 1.1 bar and the highest crossflow velocity. The filtered beer quality parameters, such as haze, color, proteins, polyphenols and bitterness, were examined after 8 h of filtration to ensure the transmission of beer compounds that are essential for beer quality. The results of quality analysis showed that the ceramic membrane crossflow filtration, regardless of very low permeation flux, appears to be a reliable substitution for the traditional Kieselguhr filtration in beer clarification.

Keywords: Microfiltration; Membrane fouling; Beer; Crossflow; Classical model

1. Introduction

Membrane separation processes, including microfiltration, ultrafiltration, and nanofiltration, can be a good substitution for conventional concentration, separation, and purification techniques in the food industry. Crossflow microfiltration of rough beer (RB) has been attracting a great research interest in recent years. This increasing interest toward application of

*Corresponding author.

membranes in brewing industry is attributed to the fact that the membrane separation process involves no phase changes and chemical agents [1] and also provides additional advantages in quality, environmental, simplicity, flexibility, and cost [2,3]. Moreover, microfiltration can provide clarification, stabilization, and sterilization in one single continuous operation [4]. However, industrial application of membranes in brewing process has been limited by membrane fouling and subsequent dramatic reduction in permeate flux even one to three orders of magnitude lower than the initial flux [5]. This low flux which is obtained in beer microfiltration rather than other beverages, such as wine and fruit juice, may be due to the high beer content of proteins and carbohydrates [6,7]. Flux decline during crossflow microfiltration of RB suspensions can be caused by several factors including (i) concentration polarization; (ii) compact cake layer formation by yeast cells, debris, and coagulated materials on membrane surface; (iii) partial or complete plugging of pore entrances by suspended particles; and (iv) adsorption of macromolecules onto the pore walls which causes the membrane pore narrowing. The membrane clogging reduces productivity and has a negative effect on membrane lifetime. Therefore, minimization of these phenomena is essential for membrane separation in order to make the process economically acceptable.

Crossflow microfiltration of beer by membranes requires a finely balanced retention of large particles (yeast cells, chill haze flocs, etc.) and transmission of carbohydrates, proteins, flavor, and color compounds, which are essential for beer quality [9]. Among these compounds, proteins and carbohydrates are identified as key membrane foulants [10]. The fouling caused by these substances is a complex phenomenon that is dependent on many factors, including the geometry and pore size distribution of the membrane [11], porosity and interconnectivity [12], pH of the solution [13], feed concentration [12] and operating parameters, such as crossflow velocity, transmembrane pressure, and temperature [14].

There have been numerous studies on the mechanisms of membrane fouling in crossflow microfiltration of suspensions containing proteins and other macromolecules [15–18]. Several attempts have been made to minimize fouling and make the beer microfiltration more efficient. Stopka et al. [19] investigated the flux decline during microfiltration of a beer sample by two different pore size ceramic membranes and found that a 500 nm membrane exhibited a lower steady-state flux but a better beer quality compared with that was obtained by a 200 nm membrane. Also they showed that a mild backflushing with a frequency up to $2\,min^{-1}$ increased the steady-state flux by 60%. Yazdanshenas et al. [20] studied the effect of different pore sizes in clarification of rough non-alcoholic beer (RNAB). They used a polymeric membrane with pore sizes of 0.2, 0.45, 0.8, and 1.2 μm and concluded that rejection for all components in RNAB increased with smaller pore sizes. Gan [21] studied the crossflow microfiltration of beer suspension by a ceramic membrane and compared various methods of flux enhancement techniques. He found that the pore entrance blockage and in-depth particle clogging were the main reasons of membrane fouling. He suggested that the backflush technique was the most effective method which led to increase 410% in steady state permeation flux. Fillaudeau and Carrerè [8] evaluated the impact of beer composition and also the mean pore diameter of various ceramic membranes on fouling and retention of particles during crossflow microfiltration of beer. They concluded that the predominant fouling mechanism for RB filtration was the yeast cell layer formation on the external surface of membrane. They proposed an empirical correlation with calculate the cake resistance at steady-state condition as functions of crossflow velocity and transmembrane pressure. Also, they concluded that the fouling mechanism was dependent on the membrane pore size and membranes with smaller pores were fouled due to the internal adsorption of proteins, polyphenols and carbohydrates while formation of a thin yeast layer governed the flux decline for large-pore-membranes. Blanpain-Avet et al. [22] proposed a study on the fouling mechanism and protein rejection for microfiltration of clarified beer (CB) through a 0.2 μm polycarbonate membrane. They figured out that the standard blocking model (SBM) conformed to the experimental data at the early stage of microfiltration and after that the cake filtration law applied to the end of the experiments. Also they noted that the build up of a compact, compressible layer on the membrane was responsible for the loss of essential quality components of beer.

Despite these extensive studies, however, the phenomenology of fouling mechanisms is still undefined and selection of an appropriate technique for flux enhancement in crossflow microfiltration of beer requires a detailed understanding of the causes of membrane fouling and also the contribution of each cause. In this study, the effects of varying operating conditions on the use of Hermia's model [23] in crossflow microfiltration of DME and also CB are investigated. Filtration pressure, crossflow velocity, and the process temperature were varied in a wide range (0.2–2.2 bar, 0.025–1.1 m/s and 3.5–17.3°C, respectively) to determine the influence of each operating parameter

on the fouling mechanisms proposed by Hermia in the microfiltration of beer suspensions. Furthermore, the quality of the collected permeate in 8 h was compared with initial feed to check the applicability of ceramic membranes in brewing industry.

2. Fouling models

To better understand the fouling characteristics during crossflow microfiltration of RB suspensions and to identify the key mechanisms that govern the process, the well-known Hermia impirical model is employed. This model corresponds to four basic types of fouling mechanisms: cake layer formation, intermediate blocking, standard blocking, and complete blocking. All these models for flux decline during constant pressure filtration process can be summarized by a single mathematical expression as follows:

$$\frac{d^2t}{dV^2} = K\left(\frac{dt}{dV}\right)^n \tag{1}$$

In this equation, t is the filtration time, V is the cumulative filtrate volume, K is the proportionality constant, and the exponent n represents the fouling model and takes different values for each type of fouling mechanism.

For the cake filtration model (CFM), the exponent n is equal to zero. According to this model, a cake layer is formed on the membrane surface because the solute molecules and solid particles are larger than membrane pores and do not penetrate inside the pores (Fig. 1(a)). Under this condition, the accumulation of particles on the membrane due to permeate drag force can lead to formation of a stagnant cake layer which is permeable to fluid flow. The relation between the permeation flux and filtration time for CFM can be expressed as follows:

$$J = J_0(1 + 2K_c(AJ_0)^2t)^{-0.5} \tag{2}$$

where K_c is the CFM constant, and J_0 is the initial flux that depends on transmembrane pressure, permeate viscosity and intrinsic membrane resistance. The linearization of Eq. (2) results in Eq. (3):

$$J^{-2} = J_0^{-2} + k_c t \tag{3}$$

where $k_c = 2K_cA^2$ and is assumed to be a constant value for constant pressure filtration.

For the intermediate blocking model (IBM), the exponent n is equal to 1. In this model, a solute particle may block a pore on the membrane surface or may deposit on another particle when it approaches the membrane. This means that not every particle blocks a membrane pore when arrives the membrane surface (Fig. 1(b)). Intermediate blocking usually accrues when the particle size is similar to the membrane pore size. The time-dependent permeate flux for this model can be written as follows:

$$J = J_0(1 + K_iAJ_0t)^{-1} \tag{4}$$

Eq. (4) can be linearized to obtain Eq. (5):

$$J^{-1} = J_0^{-1} + k_i t \tag{5}$$

In this equation, k_i is constant and is equal to K_iA. This parameter represents the blocked membrane surface per unit of the total volume that penetrates through the membrane [24]. Since the membrane area that is not blocked reduces with time, the probability of a solid particle to block a pore also decreases with time [25].

For the SBM, the exponent n is equal to 1.5. This fouling model can occur when the solute or solid particles are smaller than the membrane pore size. So they can be adsorbed into the membrane pore walls and decrease the pore volume (Fig. 1(c)). For this model, the permeate flux with time is given by:

$$J = J_0\left(1 + \frac{1}{2}K_s(AJ_0)^{0.5}t\right)^{-2} \tag{6}$$

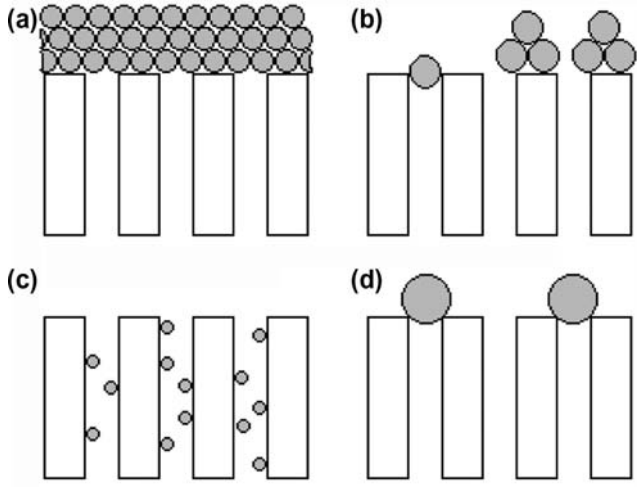

Fig. 1. Different fouling mechanisms considered by the models: (a) cake layer formation; (b) intermediate blocking; (c) standard blocking and (d) complete blocking.

The linearized form of Eq. (6) results in Eq. (7).

$$J^{-0.5} = J_0^{-0.5} + k_s t \tag{7}$$

The parameter k_s is constant and is equal to $k_s = 1/2K_sA^{0.5}$. In this model, it is assumed that all pores have a constant diameter and length along the membrane [24].

For complete blocking model (CBM), the exponent n is equal to 2. According to this model, each particle that reaches the membrane blocks the pore entrance completely and also this particle never settles on another deposited particle (Fig. 1(d)). Based on this model, the permeate flux vs. time can be explained by Eq. (8):

$$J = J_0 e^{-k_b t} \tag{8}$$

Eq. (8) can be linearized to Eq. (9):

$$\ln(J^{-1}) = \ln(J_0^{-1}) + k_b t \tag{9}$$

The parameter k_b is the model constant and is a function of blocked membrane surface per unit of the total permeate volume.

Therefore, plotting the left hand side of the linearized form of flux vs. filtration time can define which model is consistent during cross flow microfiltration of beer suspension. For each set of experimental data, fitting of the four models to experimental data was carried out and the model rate constants were calculated from the slope of the fitted line. Comparing the correlation coefficient obtained in fitting of each model, the best suited fouling model was selected in crossflow microfiltration of the beer samples.

3. Experimental

The experiments were conducted in a crossflow microfiltration pilot plant (Fig. 2). A feed tank of 19.5 L capacity was equipped to store the feed slurry. The particle size distribution of the feed suspension was measured using Laser Light Scattering (CILAS®, model 1064 Liquid, range: 0.04–500 m). A rotary vane pump (Fluid-o-Tech®, 3504, Italy) was used to pump the feed through the filtration unit. The feed temperature was kept constant by passing it through a long narrow tube which was situated in a cool constant-temperature water bath.

The pressurized feed flows tangentially across a ceramic membrane with nominal pore size of 0.45 μm. The materials used in the membrane are a combination of silica and aluminum oxides. The feed temperature and pressure were measured by two integrated sensors (Haffmans®, RPU353, The Netherlands) with accuracies of ±0.25°C and ±0.08 bar, respectively. The average feed flow rate was determined by a rotameter (Azmoon Motamam®, RGD4, Iran) with a precision of ±8 L/h. The average crossflow velocity was then calculated by dividing the feed flow rate by the channel cross-sectional area. In the cases where the permeation rate was high (pure water or CB), the permeate flow rate was measured by a rotameter (Azmoon Motamam®, RGD2, Iran, precision ±2 L/h); otherwise, it was measured using a digital balance (Sartorius®, GP 5202, Germany) with an accuracy of ±0.1 g.

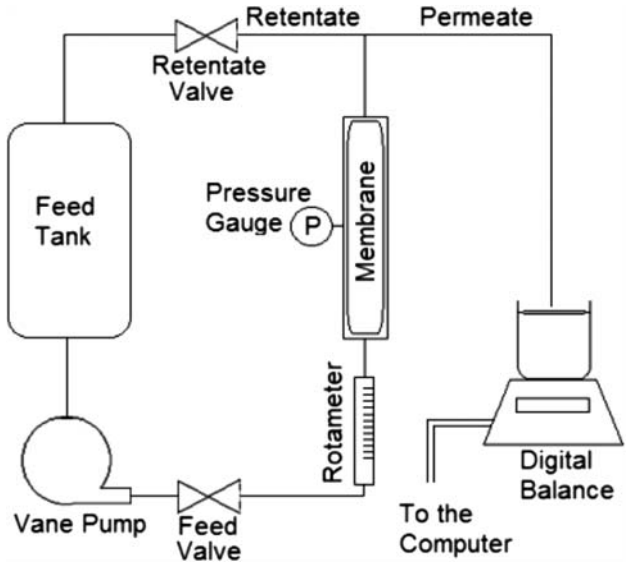

Fig. 2. Schematic representation of the laboratory setup.

The instruments' characteristics and their applications are summarized in Table 1.

Then, the permeation flux can be evaluated by the following equation:

$$J = \frac{1}{\rho g A}\frac{\mathrm{d}W}{\mathrm{d}t}$$

where ρ is the permeate density, A is the membrane surface area, and W is the permeate weight which was transferred to a computer every 0.4 s. The feed flow rate and transmembrane pressure were controlled by manipulating the feed and retentate valves, respectively. The crossflow velocity was adjusted to a range of 0.025–1.091 m/s by changing the internal tube fitted to the inside of the module and the feed flow rate was kept at a constant value (300 L/h). To clean the fouled membrane after each run, the loop was emptied and washed with water at temperature of

Table 1
The instruments' characteristics and their applications in the microfiltration pilot plant

Instrument	Details	Application
Feed tank	19.5 Liter	Feed storage
Rotary vane pump	Fluid-o-Tech®, 3504, Italy	Feed circulation
Rotameter	Azmoon Motamam®, RGD4, Iran, precision ± 8 L/h	Measuring average feed flow rate
Digital balance	Sartorius®, GP 5202, Germany, accuracy ±0.1 g	Measuring low permeate flux
Rotameter	Azmoon Motamam®, RGD2, Iran, precision ±2 L/h)	Measuring high permeate flux (CB or pure water)
Membrane	Atlas Filtri®, AB10-VSX0.45mcr, Italy, $L = 0.208$ m, $\varphi_{int/ext} = 0.032/.0048$ m, external filtration area = 0.0314 m^2	Prevent passage of particles
Scanning electron microscopy	Philips® XL30	Visual perception of the membranes and fouling structure
Mercury intrusion test	POROTEC®, Pascal 440, ISO 15901-1:2005	Determination of membrane pore size distribution
Integrated sensors	Haffmans®, RPU353, the Netherlands	Measuring the feed temperature and pressure
Module shell	Plexiglas®, $\varphi_{int} = 80$ mm	Changing flow cross- sectional area – membrane observation

about 20°C. The membrane was then backwashed by 2% sodium hydroxide solution at 75°C for about 10 min. For the cases in which the membrane resistance was beyond 10% of a new membrane resistance, the cleaning procedure was repeated with 1% phosphoric acid or 0.5% NaClO solution. The effectiveness of cleaning was checked by comparing the cleaned membrane resistance with the initial membrane resistance.

4. Results and discussion

In this work, Hermia's empirical models were used to investigate the fouling phenomena occurring in the microfiltration of nonalcoholic beer suspension. The fitting of experimental flux data to the linearized forms of these models allows us to know if the permeate flux decline is controlled by the internal fouling of the membrane or the cake layer formation. Two types of feed solution with different concentrations were used for this purpose. The first one was CB which was completely free from alcohol. The main reason to use this type of feed was that the concentration polarization and cake layer formation could be assumed to be negligible. Thus, it was possible to study the internal fouling of the membrane. The pasteurization of CB is an example of the application of CB microfiltration which is essential to obtain the microbiological stability of the final beer product. The other feed was dilute malt extract (DME) which had a higher amount of suspended solids dispersed into it which has the potential to generate a cake layer on the membrane surface. The physical properties of the feeds are listed in Table 2.

The particle size distribution of DME suspension is depicted in Fig. 3. Analysis of size distribution revealed that the particle counts peaked at 112 μm and the average particle size was 96 μm. The plot shows that about 99% of the solid particles are larger than 1 μm. This type of feed has the potential to make a cake layer due to the containing high amounts of large particles that were greater than the membrane nominal pore size (0.45 μm).

Fig. 4 shows a plot of $\ln(d^2t/dV^2)$ vs. $\ln(dt/dV)$ for microfiltration of DME and CB suspensions. The first and second derivatives were calculated by numerical differentiation. Fitting a straight line to the experimental data, one can observe from Fig. 4(a) that the best fit is obtained for $n = 1.53$ for CB suspension.

Table 2
Feed properties

Property	CB sample	DME sample
Chill haze (EBC)	1.2 ± 0.1	284.9 ± 0.1
Brix	3.8 ± 0.1	3.8 ± 0.1
Color (EBC)	4.8 ± .01	14.5 ± 0.1
pH	4.1 ± 0.1	5.1 ± 0.1
Density (kg/m^3)	1,050 ± 20	1,089 ± 20

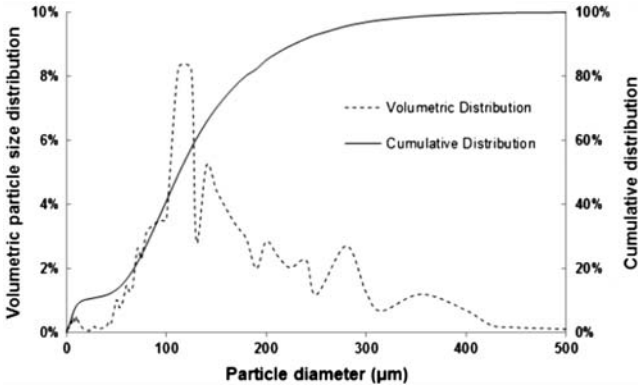

Fig. 3. Volumetric and cumulative distribution of particle diameter of DME (Haze = 284 EBC, pH=5.2).

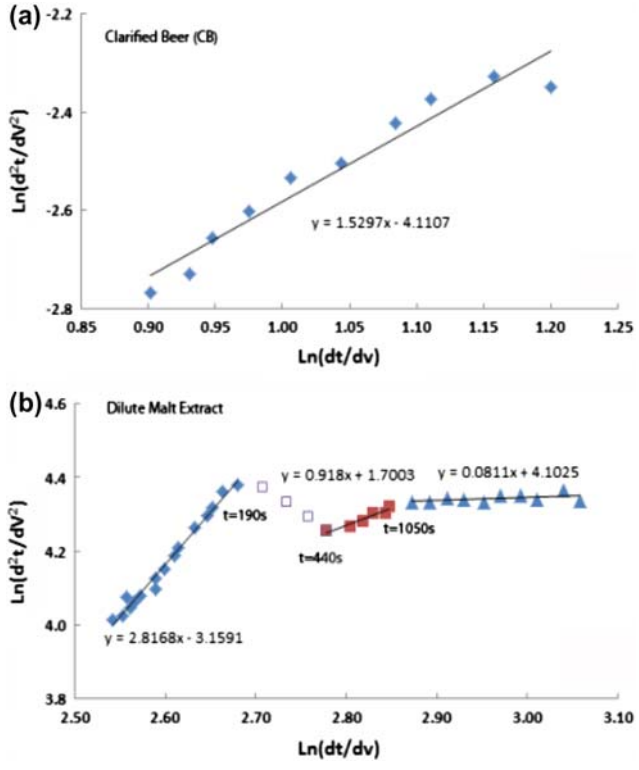

Fig. 4. Analysis of crossflow microfiltration flux decline for (a) CB, TMp = 0.5 bar, CFV = 0.85 m/s, T = 7.1 °C and (b) DME, TMp = 1.1 bar, CFV = 0.9 m/s, T = 3.5 °C.

This suggests that the standard blocking is the dominant fouling mechanism for crossflow microfiltration of CB, as was expected. According to the SBM, solute molecules can enter completely into the membrane pores and they can be adsorbed onto the membrane pore walls. However, the characteristic curve shows a different behavior for DME suspension.

According to Fig. 4(b), the characteristic curve started to increase with a slope even steeper than that of complete pore blocking model at the first 190 s ($n > 2$). This can be related to the irregular interconnections of the membrane pore structures [26]. After that, the curve begins to descend. This trend may describe a transition in fouling mechanism from CBM to IBM [26,27] in the range of 190 and 440 s. After that, a subsequent increase with a slope of about 0.92 was observed in characteristic curve which indicates that the process is followed by the intermediate pore blocking of the membrane pores. In this condition, solute particles can deposit on the other particles that previously were deposited and blocked the membrane pores. The deposition of particles on the others continues until a cake layer is formed over the membrane surface at 1,050 s. Thereafter, the formation of a cake layer and accumulation of particles on the membrane surface controls the flux in crossflow microfiltration of DME suspension. This can be seen in Fig. 4(b) where the slope of the characteristic curve drops to 0.08.

To verify the fact that the internal blocking of membrane pores is the main fouling mechanism in crossflow microfiltration of CB and that the cake formation is the main factor that governs DME filtration, the experiments were carried out at various crossflow velocities for these two types of feed. It was observed that increasing the feed flow rate at a constant transmembrane pressure had only a negligible effect on the permeate flow rate of CB (Fig. 5(a)).

This means that no cake layer was formed during microfiltration of CB solution and the dominant fouling mechanism was the internal fouling of the membrane due to the adsorption of macromolecules and other colloids into the membrane pores. However, it can be seen from the Fig. 5(b) that for DME filtration, increasing the crossflow velocity improved the flux which implies that a cake layer was formed and provided a secondary resistance to the permeate flow and caused a reduction in permeation flux. In fact, increasing the fluid velocity correspondingly increases the wall shear stress which causes the erosion of the formed cake and enhancement of steady-state flux [28,31]. A maximum value of 20 LMH was obtained at medium transmembrane pressures (1.1 bar) and the highest crossflow velocity [32]. In a limiting case where the crossflow velocity approaches zero (dead-end filtration), the steady-state flux appears to reach an asymptotic value of 6 LMH. This relatively low flux can explain why the microfiltration of beer is preferred to be conducted in a crossflow configuration rather than dead-end one.

The steady-state flux is an important parameter for industrial membrane applications. The dependence of

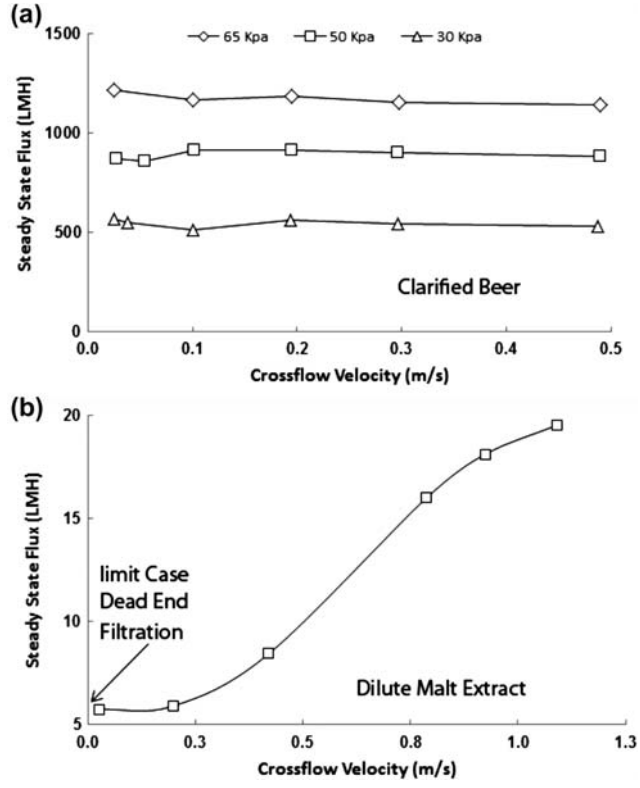

Fig. 5. Effect of crossflow velocity on steady-state permeation flux for (a) CB (TMp = 30, 50, and 65 kPa) and (b) DME, (TMp = 1.1).

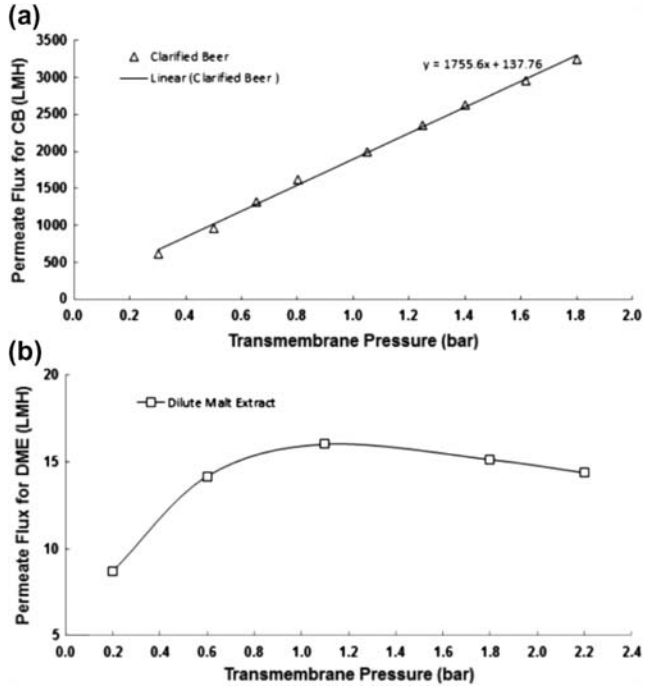

Fig. 6. Effect of transmembrane pressure on steady-state permeate flux for microfiltration of (a) CB at T = 7.1 ˚C, CFV = 0.9 m/s and (b) DME at T = 3.5 ˚C, CFV = 0.85 m/s.

steady-state permeation flux to the filtration pressure for two types of feed is compared in Fig. 6.

It can be seen in Fig. 6(a) that increasing the filtration pressure results in a higher permeation flux for CB suspension, while it does not necessarily improve the flux for DME microfiltration. As is apparent from Fig. 6(b), increasing the transmembrane pressure up to 1.1 bar enhances the flux. Any further increase in filtration pressure results in a decrease in steady-state flux. This is in good agreement with Blanpain-Avet et al. [22] who found the transmembrane pressure of 1 bar to be a critical pressure above which fouling resistance increased abruptly for beer microfiltration. The reduction in steady-state permeation flux with transmembrane pressure clearly reveals the compressible nature of the formed cake which becomes more resistant and less porous with increasing applied pressure. In addition, more number of particles can be deposited on the membrane at higher transmembrane pressures and generate a thicker cake accordingly. Hence, the cake compression and thickening may occur simultaneously by raising the transmembrane pressure that can reduce the flux.

Fig. 7(a) represents the variation of dimensionless permeation flux with time for two different transmembrane pressures. As is evident from the figure, during microfiltration of CB, the flux decreases gradually with time. This decline in the permeate flux can be due to the narrowing of membrane pores which is caused by the adsorption of macromolecules, such as proteins and carbohydrates, within the pore walls [10]. It can also be seen that the experimental dimensionless flux versus time at 50 and 65 kPa exhibits a similar behavior. On the contrary, the dimensionless flux versus time reduces with pressure for clarification of DME. The permeate flux at different transmembrane pressures for DME is shown in Fig. 7(b).

The flux decreases drastically within the first few minutes of DME microfiltration and in some cases reached about even 1% of the initial flux. This implies an extra intensive and severe fouling of the ceramic membrane which can be attributed to the presence of protein and polyphenol compounds in DME. These two substances can combine and react to form colloidal complexes that are insoluble at the low temperatures and can precipitate to make a compact low-permeable layer. During the microfiltration of DME, large particles can approach the membrane and cause a rapid blocking of the membrane pores on the surface. Subsequently, other particles can settle on previously deposited particles which may result in

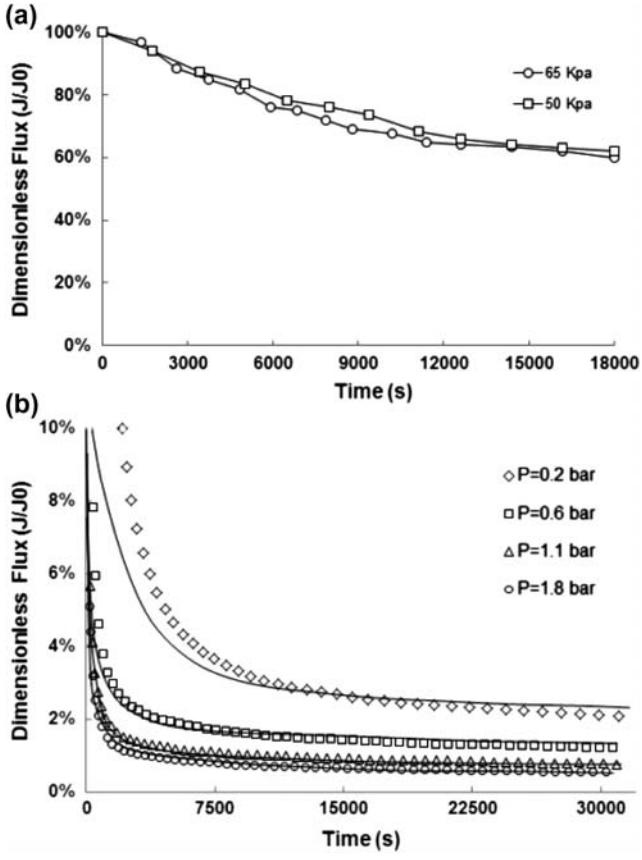

Fig. 7. Dimensionless flux vs. time at different transmembrane pressures during crossflow microfiltration of (a) CB at $T = 7.1$ ℃, CFV = 0.9 m/s and (b) DME at $T = 3.5$ ℃, 0.85 m/s, solid lines represent the cake filtration model prediction.

forming a cake layer. This layer creates a second barrier to the permeate and reduces the flux.

Table 3 summarizes the measures of fitness to the experimental data obtained in the microfiltration pilot plant for Hermia's models. It is apparent that the CFM is in the best agreement with experimental data except at very low crossflow velocities. The cake formation occurs when suspended particles are much greater than the membrane pore size and they cannot enter the membrane pores so that the retained particles accumulate at the membrane surface and form a fouling layer.

Analysis of the experimental data with CFM represents a good agreement with correlation coefficient of more than 90%. It should be noted that not always a higher value of R^2 corresponds to the best fit of a model for different operating conditions [29]. In other words, it is adequate to compare the values of R-squared for different Hermia's models and the same experimental conditions, while comparing these values for different experimental conditions and the same model does not lead to a reliable result [30].

The measured permeate fluxes vs. time for crossflow velocities of 0.025 and 1.1 m/s are shown in Fig. 8. As can be seen in Fig. 8(a), the best fit to experimental data at crossflow velocity of 0.025 m/s corresponds to the IBM, while at 1.09 m/s, the cake formation is responsible for flux decline (Fig. 8(b)). This is supported by greater regression coefficients (see Table 2). At a low crossflow velocity, the drag force exerted on fine particles toward the membrane is higher than the sum of forces due to shear induced

Table 3
The values of correlation coefficients R^2 obtained by fitting of experimental data to the Hermia's models for DME at different operating conditions (These values were obtained for 8 h of DME microfiltration)

Pressure (bar)	Temperature (℃)	Crossflow velocity (m/s)	Cake filtration	Complete blocking	Intermediate blocking	Standard blocking
0.2	3.5	0.853	0.9750	0.6581	0.8865	0.7914
0.6	3.5	0.787	0.9058	0.4225	0.7463	0.6037
1.1	3.5	0.787	0.9098	0.3945	0.7397	0.5848
1.8	3.5	0.853	0.9269	0.3988	0.7668	0.6114
1.1	3.5	0.197	0.9898	0.6073	0.9678	0.8531
1.1	9.3	0.197	0.9823	0.6463	0.9784	0.8775
1.1	17.3	0.197	0.9945	0.5693	0.9579	0.8289
1.1	3.5	0.025	0.9368	0.6279	0.9912	0.8895
1.1	3.5	0.197	0.9898	0.6073	0.9678	0.8531
1.1	3.5	0.42	0.9583	0.4901	0.8358	0.6992
1.1	3.5	0.787	0.9098	0.3945	0.7397	0.5848
1.1	3.5	0.923	0.9104	0.3885	0.7411	0.5856
1.1	3.5	1.091	0.9021	0.3312	0.7136	0.5414

and inertial lift forces acting on particles in opposite direction. So that some fine particles can approach the membrane surface easily and deposit within larger membrane pores. Also it can be observed that the SBM overpredicts the flux, while CBM underpredicts the permeate flux which was occurred for all experiments. It is also worth mentioning that the highest deviation between experimental and predicted flux was observed for the same operating conditions as in the case of the CBM (Table 2).

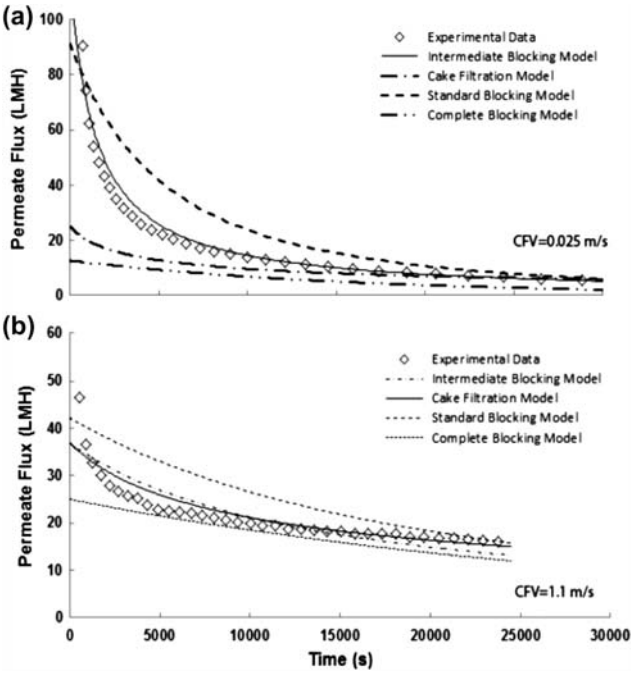

Fig. 8. Comparison between different fouling mechanisms in prediction of flux decay during microfiltration of DME at (a) CFV = 0.025 and (b) CFV = 1.1 m/s.

Table 4
Contribution percentage of each resistance in crossflow microfiltration of DME at the steady-state condition

	TMp = 0.8 bar (%)	TMp = 1.1 bar (%)	TMp = 1.8 bar (%)
Membrane resistance	4.56	13.42	1.43
Internal fouling resistance	16.82	7.42	2.40
Cake layer resistance	78.62	79.16	96.17

Table 4 lists the values of different resistances for three different transmembrane pressures and the same temperature and crossflow velocity in microfiltration of DME. The contributions of the reversible and irreversible fouling were defined by comparison of hydraulic resistances after water rinsing, water backwashing, and chemical cleaning of the fouled membrane. The results clearly indicate that the cake resistance is the largest portion of the total resistance and the irreversible resistance has low impact on the flux reduction. The total resistance, R_{tot}, was obtained by knowing the permeation flux at the steady-state condition and using Darcy's law. The membrane resistance, R_m, was measured by distilled water before each run. After the experiments, the membrane was backwashed with water to remove the stagnant layer sticked to the membrane. The internal fouling resistance, R_{irrev}, was the measured by repeating the experiment with pure water. The cake resistance, R_{rev}, was afterward obtained by subtracting the total resistance from the sum of the membrane and internal fouling resistance.

The formation of a compact cake layer during microfiltration of DME caused a flux decline and changes in membrane selectivity. This severe layer can hinder the transmission of essential beer components which had an adverse effect on permeate quality [22]. Table 5 summarizes the color, bitterness, and haze compounds of DME feed and permeate collected over 8 h of three typical filtration experiments. The pH of the solution was little affected by the membrane. The substantial protein rejection of 25% and polyphenol rejection of 35% were observed which can be related to the build up of a cake layer partially permeable to the high molecular weight solutes in beer.

Table 5
Essential beer quality compounds in feed and collected permeate during 8 h of microfiltration

	Color (EBC)	Polyphenols (mg/L)	Sensitive Protein (EBC)	Haze (EBC)	Bitterness (BU)	pH
Feed	14.50	62.4	26.3	284.9	12.5	5.1
Permeate 1	11.05	39.8	19.1	0.76	11.4	5.2
Permeate 2	11.24	41.2	20.3	0.81	11.2	5.2
Permeate 3	11.17	40.3	19.8	0.78	11.3	5.2
Removal %	23.1	35.2	24.9	99.7	9.6	–
EBC standard	11.5	–	–	<0.8	16.1	4.1

Also, a 23% reduction in feed color and 9.6% in feed bitterness was achieved by using the ceramic membrane.

Analysis of these results indicates that the ceramic membrane had a good selectivity toward the valuable and nutritional beer compounds. The outstanding property offered by the 0.45 μm ceramic membrane was being successfully able to remove almost 99.7% of haze compounds. However, the retained particles would generate significant fouling potential on membrane. It can be inferred from Table 5 that crossflow ceramic membrane separation had an acceptable performance in transmission of essential beer compounds and retention of solid particles and solutes responsible for haze. However, the low permeation flux is the main factor that should be considered in application of membranes in brewing industry.

5. Conclusion

Fouling of ceramic membranes during microfiltration of beer is severe, complex and unavoidable due to chemical diversity and large size range of compounds. The application of crossflow microfiltration in clarification of DME and also pasteurization of CB was investigated in a pilot plant consisting of a tubular ceramic membrane with nominal pore diameter of 0.45 μm. In the case of CB microfiltration, the flux declined gradually and reduced to 60% of the initial flux at the steady state condition. For this type of feed, the characteristic curve showed that the adsorption of macromolecules within membrane pores was the predominant fouling mechanism. Also, the turbidity of CB reduced by 60% from 0.5 to 0.2 EBC by applying 0.45 μm ceramic membrane. For DME clarification, the flux dropped suddenly in the first few minutes of experiment and reached about 2% of initial flux due to sever fouling of the membrane. To define the fouling mechanisms for DME microfiltration, the experimental results of flux versus time were compared with the Hermia's fouling models and the best fit to the linearized forms of equations was found to the CFM for most of the filtration. All the values of R^2 were higher than 0.9 and a good agreement was observed between the model and experimental results. For all of the experimental conditions, the fitted initial flux obtained by the intercept of fitted line was lower than the measured initial flux. The models underpredicted the initial flux. The highest steady-state flux of about 20 $Lm^{-2}h^{-1}$ was obtained at 1.1 bar and the highest crossflow velocity. The effect of transmembrane pressure on steady-state permeate flux was studied and it was found that the moderate pressures (about 1 bar) were the best choice for beer microfiltration. The filtered beer quality was also checked and found that the permeate color was reduced by 22% compared with the initial beer color and the ceramic membrane succeeded to remove almost higher than 99.7% of haze compounds without any significant reduction in essential beer components and the beer taste in all experiments, which is highly demanded by the industry. These results indicate that regardless of a dramatic reduction in permeate flux and sever membrane fouling, which can be minimized by employing proper hydrodynamic techniques, ceramic membrane crossflow filtration appears to be a feasible substitution for the traditional Kieselguhr filtration in beer clarification.

Acknowledgment

The authors are greatly indebted to Iran Behnoush Co. for the beer samples and financial support of this project.

Notation

A	—	membrane surface area, m^2
G	—	gravitational acceleration, $m\,s^{-2}$
J	—	permeate flux, $m\,s^{-1}$
J_0	—	initial permeate flux, $m\,s^{-1}$
K	—	proportionality constant in Eq. (1)
k_b	—	complete blocking model (CBM) constant, s^{-1}
K_c	—	cake filtration model (CFM) constant, $m^{-6}s$
K_i	—	intermediate blocking model (IBM) constant, m^{-3}
K_s	—	standard blocking model (SBM) constant, $m^{-1.5}\,s^{-0.5}$
N	—	exponent in Eq. (1) which depends on fouling model
R_{irrev}	—	irreversible resistance, m^{-1}
R_m	—	membrane resistance, m^{-1}
R_{rev}	—	reversible resistance, m^{-1}
T	—	time, s
V	—	accumulated permeate volume, m^3
W	—	accumulated permeate weight, kg
ρ	—	permeate density, $kg\,m^{-3}$

References

[1] A. Cassano, L. Donato, E. Drioli, Ultrafiltration of kiwifruit juice: Operating parameters, juice quality and membrane fouling, J. Food Eng. 79 (2007) 613–621.
[2] L. Fillaudeau, P. Blanpain-Avet, G. Daufin, Water, wastewater and waste management in brewing industries, J. Clean. Product. 14 (2006) 463–471.
[3] T.R. Noordman, C. Peet, W. Iverson, L. Broens, S.v. Hoof, Cross-flow filtration for clarification of lager beer economic reality, Tech. Q. Master Brew. Assoc. Am. 38 (2001) 207–210.
[4] G. Trägårdh, New developments in membrane processing, in: A.G. Gaonkar (Ed.), Food processing: Recent developments (Chapter 6), Elsevier, Amsterdam, 1995.

[5] D.Y. Kwon, S. Vigneswaran, A.G. Fane, R.B. Aim, Experimental determination of critical flux in cross-flow microfiltration, Sep. Purif. Technol. 19(3) (2000) 169–181.
[6] H.C. Van Den Horst, J.H. Hanemaaijer, Cross-flow microfiltration in the food industry: State of the art, Desalination 77 (1990) 235–258.
[7] K.J. Burrell, C. Gill, M.T. McKechnie, J. Murray, Advance in separation technology for the brewer: Ceramic cross-flow microfiltration of rough beer, MBAA Tech. Q. 31(2) (1994) 42–50.
[8] L. Fillaudeau, H. Carrerè, Yeast cells, beer composition and mean pore diameter impacts on fouling and retention during cross-flow filtration of beer with ceramic membranes, J. Membr. Sci. 196 (2002) 39–57.
[9] Q. Gan, J.A. Howell, R.W. Field, R. England, M.R. Bird, C.L. O'Shaughnessy, M.T. MeKechinie, Beer clarification by microfiltration—product quality control and fractionation of particles and macromolecules, J. Membr. Sci. 194 (2001) 185–196.
[10] A.K Pabby, A.M Sastre, S.S.H Rizvi, Handbook of Membrane Separation: Chemical, Pharmaceutical, Food and Biotechnological Applications, CRC, New York, NY, 2008.
[11] M. Chandler, A. Zydney, Effects of membrane pore geometry on fouling behavior during yeast cell microfiltration, J. Membr. Sci. 285(1–2) (2006) 334–342.
[12] L. Palacio, C.C. Ho, P. Prádanos, A. Hernández, A.L. Zydney, Fouling with protein mixtures in microfiltration: BSA-lysozyme and BSA-pepsin, J. Membr. Sci. 222(1–2) (2003) 41–51.
[13] C. Velasco, M. Ouammou, J.I. Calvo, A. Hernández, Protein fouling in microfiltration: Deposition mechanism as a function of pressure for different pH, J. Colloid Interf. Sci. 266(1) (2003) 148–152.
[14] G. Samuelsson, P. Dejmek, G. Trägårdh, M. Paulsson, Minimizing whey protein retention in cross-flow microfiltration of skim milk, Int. Dairy J. 7(4) (1997) 237–242.
[15] H.W. Sur, Z. Cui, Experimental study on the enhancement of yeast microfiltration with gas sparging, J. Chem. Technol. Biotechnol. 76(5) (2001) 477–484.
[16] C.J. Chuang, C.Y. Wu, C.C. Wu, Combination of crossflow and electric field for microfiltration of protein/microbial cell suspensions, Desalination 233(1–3) (2008) 295–302.
[17] S.A.M. Mourouzis, A.J. Karabelas, Whey protein fouling of large pore size ceramic microfiltration membranes at small cross-flow velocity, J. Membr. Sci. 323(1) (2008) 17–27.
[18] F. Martínez, A. Martín, P. Prádanos, J.I. Calvo, L. Palacio, A. Hernández, Protein adsorption and deposition onto microfiltration membranes: The role of solute–solid interactions, J. Colloid Interf. Sci. 221(2) (2000) 254–261.
[19] J. Stopka, Š. Schlosser, Z. Dömény, D. Šmogrovičov, Flux decline in microfiltration of beer and related solutions of model foulants through ceramic membranes, Pol. J. Environ. Stud. 9 (2000) 65–69.
[20] M. Yazdanshenas, S.A.R. Tabatabaei Nejad, M. Soltanieh, A. Tavakkoli, A.A. Babaluo, L. Fillaudeau, Dead-end microfiltration of rough nonalcoholic beer by different polymeric membranes, J. Am. Soc. Brew. Chem. 68(2) (2010) 83–88.
[21] Q. Gan, Beer clarification by cross-flow microfiltration—effect of surface hydrodynamics and reversed membrane morphology, Chem. Eng. Process. 40 (2001) 413–419.
[22] P. Blanpain-Avet, L. Fillaudeau, M. Lalande, Investigation of mechanisms governing membrane fouling and protein rejection in the sterile microfiltration of beer with an organic membrane, Trans. I Chem. E 77 (1999) 75–89.
[23] J. Hermia, Constant pressure blocking filtration laws—application to power law non-newtonian fluids, Trans. Inst. Chem. Eng. 60 (1982) 183–187.
[24] W.R. Bowen, J.I. Calvo, A. Hernández, Steps of membrane blocking in flux decline during protein microfiltration, J. Membr. Sci. 101 (1995) 153–165.
[25] A.B. Koltuniewicz, R.W. Field, Process factors during removal of oil-in water emulsions with cross-flow microfiltration, Desalination 105 (1996) 79–89.
[26] A.L. Zydney, C.C. Ho, W. Yuan, B. Dibakar, D.A. Butterfield, Fouling phenomena during microfiltration: Effects of pore blockage cake filtration and membrane morphology, Membr. Sci. Technol. 8 (2003) 27–44.
[27] C.C. Ho, A.L. Zydney, A combined pore blockage and cake filtration model for protein fouling during microfiltration, J. Colloid Interf. Sci. 232 (2000) 389–399.
[28] M.C. Aubert, M.P. Elluard, H. Barnier, Shear stress induced erosion of filtration cake studied by a flat rotating disk method, determination of the critical shear stress of erosion, J. Membr. Sci. 84 (1993) 229–240.
[29] Z. Gu, Across-Sample Incomparability of R^2s and Additional Evidence on Value Relevance Changes Over Time, Carnegie Mellon University, Pittsburgh, PA, 2004.
[30] M.C.V. Vela, S.A. Blanco, J.L. García, E.B. Rodrgíuez, Analysis of membrane pore blocking models applied to the ultrafiltration of PEG, Sep. Purif. Technol. 62 (2008) 489–498.
[31] Xiaoling. Lei, Simulation and mechanisms of aeration impacts on the permeate flux in submerged membrane systems, Desalin. Water Treat. 18 (2010) 277–285.
[32] Z. Wang, Y. Cui, J. Yao, J. Chu, Y. Liang, The influence of various operating conditions on specific cake resistance in the crossflow microfiltration of yeast suspensions, Desalin. Water Treat. 1 (2009) 237–247.